TimeSqueeze: Dynamic Patching for Efficient Time Series Forecasting

Sravan Kumar Ankireddy[1] * **Nikita Seleznev**[2] **Nam H. Nguyen**[2] **Yulun Wu**[2]

Senthil Kumar[2] **Furong Huang**[3] **C. Bayan Bruss**[2]

[1]University of Texas at Austin [2]Capital One [3]University of Maryland, College Park

Abstract

Recent progress in time series forecasting has produced large foundation models with strong generalization across domains. However, many of these models rely on transformer backbones, making their effectiveness constrained by the cost of processing the input context. The quadratic computational complexity with respect to sequence length imposes a fundamental trade-off on existing designs: they must either preserve high-frequency information using point-wise embeddings, which is computationally expensive for long sequences, or employ patch-based embeddings to reduce sequence length at the risk of discarding critical temporal details. To overcome this limitation, we present TimeSqueeze, a hybrid forecasting architecture that combines the strengths of both point and patch embeddings through **dynamic time series compression**. TimeSqueeze introduces a novel two-stage hybrid representation: (1) a *lightweight state-space encoder* processes the full-resolution time series with point-wise embeddings to extract fine-grained temporal features, and (2) an adaptive patching module intelligently prunes these features using *variable-sized patches*, assigning smaller patches to information-rich regions and larger patches to redundant segments. This hybrid approach yields a variable-resolution representation that preserves critical temporal details while reducing computational overhead. By retaining the fidelity of point embeddings and the efficiency of patch embeddings, the resulting compressed sequence enables the Transformer backbone to substantially reduce the input length without sacrificing forecasting accuracy. Extensive experiments demonstrate that TimeSqueeze achieves state-of-the-art forecasting performance while delivering substantial computational advantages, including up to $8\times$ improvement in pretraining data efficiency and up to $20\times$ reduction in pretraining time compared to equivalent point-embedding models.

1 Introduction

Accurate time-series forecasting is crucial across numerous domains, including energy, finance, climate, and healthcare. Historically, forecasting has relied on narrow, task-specific statistical models; however, recent advances in deep learning have enabled the development of versatile, generalist models capable of cross-domain transfer. In particular, time-series foundation models trained on heterogeneous datasets offer flexible zero-shot and few-shot generalization across a wide range of forecasting tasks.

Effective pretraining of these foundation models necessitates modeling long historical contexts, often extending to thousands of timesteps, which creates formidable computational and memory constraints.

*Correspondence to: sravan.ankireddy@utexas.edu. Work done in part during internship at Capital One.

NeurIPS 2025 Workshop on Recent Advances in Time Series Foundation Models (BERT^{2}S).

Recent studies demonstrate that increasing context length during pretraining yields substantial improvements in downstream inference performance [1, 2]. Therefore, designing architectures that remain scalable and computationally efficient under long-context regimes is imperative for realizing the full potential of time series foundation models.

Central to addressing these scalability challenges is the design of an efficient tokenizer that effectively represents input signals in an embedding space while managing computational complexity. Current approaches predominantly adopt one of two strategies. The first approach involves independently encoding each time point [3, 4, 5, 6, 7], which preserves fine-grained temporal variations and accommodates data of arbitrary frequency and seasonality. However, this point-wise encoding strategy suffers from limited scalability as sequence length increases, which is precisely the bottleneck that impedes long-context pretraining. The second approach, pioneered by [8] and subsequently adopted by numerous transformer-based forecasting models [9, 10, 11, 2], employs fixed-size patching to compress multiple consecutive time points into a single embedding. While this patching strategy significantly enhances computational scalability, it introduces some limitations that compromise its effectiveness. First, determining the optimal patch size is non-trivial and heavily dependent on dataset-specific characteristics such as sampling frequency and seasonal patterns, typically requiring empirical evaluation across different patch sizes for each dataset. Second, and perhaps more critically, many time series exhibit heterogeneous information density across different temporal regions, with some segments displaying rapid variations while others remaining relatively stable. This temporal heterogeneity renders uniform patching suboptimal, as it fails to adapt the representational granularity to the local complexity of the signal.

$_{o}ld$

Motivated by these requirements, we propose TimeSqueeze, a hybrid time-series foundation model that combines the expressive power of point-embeddings with the computational efficiency of patch-embeddings. First, a lightweight state-space encoder extracts local fine-grained features at full resolution. Then, a dynamic patching module groups these embeddings into patches of varying sizes, allocating smaller patches to information-rich regions and larger patches to redundant ones, yielding a variable-resolution representation. This compressed sequence is processed by a Transformer backbone, which operates on significantly fewer tokens while preserving salient temporal dynamics, thereby overcoming fixed patch size limitations and enabling scalable, high-fidelity modeling.

Our contributions are as follows:

- We propose TimeSqueeze, the first hybrid forecasting architecture to incorporate dynamic, content-aware patching for adaptive compression in time series.
- We demonstrate that TimeSqueeze integrates seamlessly with existing Transformer backbones (e.g., Time-MoE), enabling pretraining of large-scale time series foundation models with substantially reduced training budgets.
- We validate TimeSqueeze across diverse zero-shot forecasting benchmarks, achieving performance on par with state-of-the-art point embedding models while delivering up to $20\times$ faster training and $10\times$ faster inference.

2 Related Works.

Long-sequence architectures. While Transformer architectures [12] have shown strong time series forecasting performance due to their expressivity and flexibility, their quadratic computational and memory complexity with respect to sequence length limits their scalability to long historical contexts. Innovations such as [13, 4, 3] have adapted Transformers for long-term forecasting, but pretraining on extremely long contexts remains challenging. Recently, time-series foundation models have demonstrated scalability to long contexts supporting arbitrary forecasting horizons, while Time-MoE [7] leveraged Mixture-of-Experts routing to enable the first billion-parameter model with tractable inference. Despite these advances, the cost of long-context pretraining remains high due to the underlying Transformer backbone. Although state space model (SSM) architectures [14] handle long contexts more efficiently, they remain underexplored for time series forecasting, highlighting the need for scalable methods for efficient long-context processing.

Patch-based compression. Introduced in PatchTST [8], patch-based compression has emerged as a fundamental technique for scaling time series foundation models. By embedding contiguous sub-

sequences (patches) rather than individual time points, this approach reduces the effective sequence length while preserving essential local temporal patterns. Subsequent foundation models, including TimesFM [10], Moment [9], Moirai [11], and Timer-XL [2], have adopted this paradigm, collectively demonstrating that patching enables more efficient training and inference. However, these approaches utilize a fixed patch size for a given sequence, limiting their application to real-world data with high temporal variance, underscoring the need for dynamic, data-driven compression strategies that can adjust patching to varying temporal structures within a series.

Insights from language modeling. Similar challenges arise in large language models (LLMs), where the choice of input representation has a direct impact on scalability and fidelity. Conventional tokenization introduces systematic biases and brittle dependencies, motivating tokenizer-free models that operate at the byte level. Yet, naïve byte-level processing leads to prohibitively long input sequences [15], straining attention-based architectures. To overcome this, adaptive compression techniques have been proposed. The Byte Latent Transformer (BLT) dynamically merges predictable byte spans into compact latent tokens using entropy-guided segmentation [16], while H-Net [17], inspired by U-Net [18] and its broad adaptation in vision [19, 20, 21], compresses and reconstructs sequences in various resolutions, and uses a state-space model for more efficient byte-level processing. These approaches highlight a key principle: efficiency and accuracy can be jointly achieved by allocating higher granularity to information-dense regions and applying more aggressive compression where redundancy dominates.

3 Methodology

Problem Statement. The fundamental objective in time-series forecasting is to predict future values based on historical observations. Given a sequence of T historical data points, $\mathbf{X}_{1:T} = (x_1, x_2, \ldots, x_T) \in \mathbb{R}^T$, the goal is to estimate the next H values of the series. This is formalized via a model f_θ that maps the historical context to future predictions, i.e., $\hat{\mathbf{X}}_{T+1:T+H} = f_\theta(\mathbf{X}_{1:T}) \in \mathbb{R}^H$. Adopting the channel independence principle of **(author?)** [8], the model can flexibly process multivariate time series by decomposing inputs into collections of univariate series. This general formulation enables time-series foundation models to address forecasting tasks with arbitrary input dimensionality, thereby supporting broad applicability across diverse, real-world domains.

3.1 Architectural Overview

To combine the expressivity of point-embeddings with the computational efficiency of patch embeddings, TimeSqueeze employs a hybrid multi-resolution architecture with four key components: (1) a lightweight encoder-decoder pair operating at full input resolution to capture fine-grained local features, (2) adaptive patching modules that dynamically select salient features for efficient downsampling and upsampling, (3) a decoder-only MoE Transformer backbone for modeling causal dependencies at scale, and (4) a multi-horizon forecasting head that jointly optimizes predictions across multiple time horizons to support both short- and long-term forecasting, as shown in Figure 1.

Formally, the end-to-end model can be described as

$$H_{1:T} = \mathcal{E}(X_{1:T}), \quad Z_{1:P} = \mathcal{M}(\mathcal{P}(H_{1:T})), \quad Y_{1:T} = \mathcal{D}(H_{1:T}, \mathcal{U}(Z_{1:P})), \tag{1}$$

where $\mathcal{E}$ is the encoder, $\mathcal{P}$ is the patching module, $\mathcal{M}$ is the MoE Transformer backbone, $\mathcal{U}$ is the unpatching module, and $\mathcal{D}$ is the decoder. Here, $X_{1:T} \in \mathbb{R}^T$ denotes the original input sequence, $H_{1:T} \in \mathbb{R}^{T \times D}$ denotes the D-dimensional encoder embeddings, $Z_{1:P} \in \mathbb{R}^{P \times D}$ denotes the patch-level latent representation after $\mathcal{P}$ and $\mathcal{M}$, and $Y_{1:T} \in \mathbb{R}^{T \times D}$ denotes the decoder embeddings that serve as the final representation for downstream forecasting.

3.1.1 State-Space Encoder and Decoder

The encoder and decoder modules operate directly on input time series at native resolution to preserve fine-grained temporal details essential for accurate forecasting, particularly in high-frequency data. To handle long, uncompressed sequences efficiently while generating representations suitable for subsequent patching, both modules are constructed using Mamba layers [14].

Mamba offers nearly linear computational scaling with respect to sequence length, enabling extraction of intricate local patterns from extended contexts by the encoder, without the quadratic complexity of

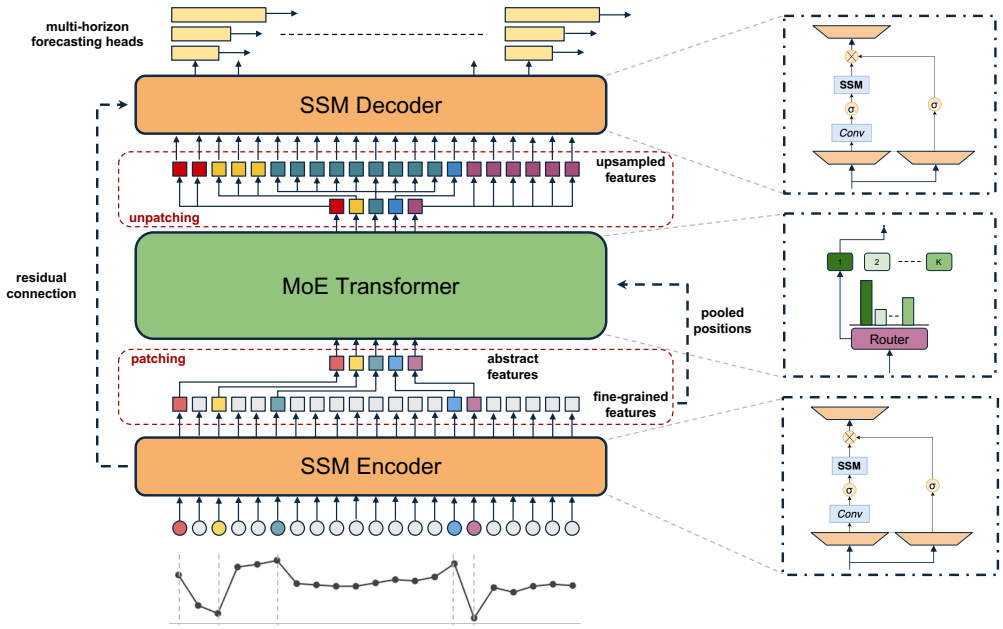

Figure 1: Architectural overview of TimeSqueeze. An SSM encoder first processes the raw series at full resolution to extract fine-grained features. Dynamic patching then adaptively compresses the sequence, selecting the salient subset of embeddings. A Transformer backbone performs contextual modeling on the downsampled features, and an unpatching module upsamples the signal to the original resolution while preserving causality. Finally, an SSM decoder combines the compressed and fine-grained features, passing the hybrid features to multi-horizon heads, thereby improving efficiency without sacrificing temporal fidelity.

traditional Transformer architectures. Further, the decoder uses the same architecture to efficiently combines outputs from the Transformer backbone with residual embeddings from the encoder to produce final representations for forecasting, creating a rich multi-scale feature space that captures both local fine-grained patterns and global contextual dependencies.

3.1.2 Dynamic Patching and Unpatching

After the encoder produces fine-grained representations, the patching module compresses the sequence of embeddings before passing them to the Transformer backbone. The objective is to allocate computational resources efficiently by employing a dynamic patching strategy that adapts to the local complexity of the input signal. This strategy forms larger patches to compress regions of low information density while using smaller patches to preserve detail in regions of high information content. A visualization of the patch boundaries for different datasets is provided in Appendix H.

Patching. Unlike language models that operate on discrete token sequences, time series data exist in continuous space and exhibit rich statistical properties. This continuous nature makes time series particularly amenable to characterization via statistical measures such as local variance or power, without relying on external metrics for guidance [16]. We leverage this by tracking the absolute difference between consecutive samples, comparing it to the average signal power within a predetermined lookback window, and then computing the patch boundaries in the original signal space rather than the embedding space. Formally, we maintain a sliding window $\mathcal{W}_i = \{x_{i-L}, \ldots, x_{i-1}\}$ of length L to compute the local average power as

$$P_i = \frac{1}{L} \sum_{j=i-L}^{i-1} x_j^2.$$

Our adaptive patching mechanism declares a patch boundary at timestep i if the absolute difference between consecutive samples exceeds a threshold scaled by the local power, which we refer to as **relative deviation-based patching**:

$$b_i = \begin{cases} 1 & \text{if } |x_i - x_{i-1}| > \tau\sqrt{P_i} \\ 0 & \text{otherwise} \end{cases}.$$

Here, $\tau > 0$ is a tunable threshold parameter controlling patch sensitivity and the average compression ratio. Using $\sqrt{P_i}$ normalizes the threshold with respect to signal amplitude, allowing the method to adapt dynamically across varying signal magnitudes and variances. Once patch boundaries are determined, the embeddings within each patch are compressed by retaining only the boundary embeddings and discarding intermediate ones (Figure 1). Note that retaining only the boundary embeddings helps preserve causality for the subsequent unpatching step.

Unpatching. The unpatching module restores the compressed embeddings to the original sequence length while maintaining causal consistency. After backbone processing of boundary embeddings, each updated embedding is repeated across all timesteps within its corresponding patch. Since boundary embeddings represent the start of each patch, the reconstructed output at timestep t depends only on inputs from times $\leq t$, preventing leakage of future information.

Positional Information. Unlike language models, which predict the next discrete token, time series forecasting models demands more nuanced objective during pretraining. Forecasting must occur at a specified frequency within the original continuous signal space, not within the compressed embedding space. Prior works on tokenizer-free language modeling, such as BLT [16] and Dynamic Chunking [17], do not retain the original positional indices and restrict the attention mechanism to relative positional information post-downsampling. In contrast, TimeSqueeze explicitly preserves the position IDs of embeddings before downsampling and utilizes these absolute positions to compute attention after compression.

3.1.3 Mixture-of-Experts Transformer Backbone

Due to its modular design, our hybrid feature extraction framework is compatible with any existing time-series forecasting backbone. In this work, we adopt the Time-MoE backbone [7], a scalable decoder-only Transformer augmented with a sparse MoE routing mechanism. Time-MoE incorporates several enhancements to improve training stability and forecast accuracy: it employs RMSNorm for layer normalization and replaces absolute positional encodings with Rotary Positional Embeddings (RoPE), facilitating better handling of variable sequence lengths and improved extrapolation. Following established design patterns, the standard feed-forward network (FFN) is replaced by an MoE layer containing a pool of N non-shared experts alongside one shared expert that consolidates common knowledge. For each input token, a routing mechanism selects the top K non-shared experts to process the signal, enabling efficient scaling to billions of parameters while maintaining manageable inference costs.

3.1.4 Multi-horizon forecasting

To enhance forecasting flexibility and robustness, we employ a multi-horizon forecasting head as introduced in [7]. This approach enables simultaneous prediction across multiple future horizons rather than restricting the model to a single forecast length. Specifically, it consists of multiple single-layer FFNs, each dedicated to a distinct forecasting horizon. The model is trained using a composite loss aggregating errors from all horizons, which improves generalization. During inference, a simple scheduling strategy selects the appropriate horizon-specific output, enabling the model to produce forecasts of arbitrary length flexibly.

3.2 Model Training

Pretraining Dataset. Efficient pretraining of a foundation model necessitates a large and diverse dataset. For this purpose, we employ the Time-300B dataset [7], a high-quality, open-access dataset composed of time series from numerous public sources across various sectors, including weather, transportation, and finance, which is further expanded with synthetic data. It consists of a broad range of frequencies, ranging from seconds to yearly, and a massive scale of over 300 billion time points, making it well-suited for pretraining large-scale models.

Loss Formulation. Following [7], our training objective is a composite loss function that combines a primary forecasting loss with an auxiliary term for load balancing, which enables a fair comparison against the point-embedding baseline Time-MoE. The primary auto-regressive loss, $\mathcal{L}_{\text{ar}}$, is the Huber Loss [22], chosen for its robustness against outliers:

$$\mathcal{L}_{ar}(x_t, \hat{x}_t) = \begin{cases} \frac{1}{2}(x_t - \hat{x}_t)^2, & \text{if } |x_t - \hat{x}_t| \leq \delta, \\ \delta\left(|x_t - \hat{x}_t| - \frac{1}{2}\delta\right), & \text{otherwise,} \end{cases} \tag{2}$$

where δ is a hyperparameter that balances the quadratic (L_2) and linear (L_1) penalties.

To ensure balanced expert utilization and prevent routing collapse, we incorporate an auxiliary loss, $\mathcal{L}_{\text{aux}}$, as proposed in [23]:

$$\mathcal{L}_{\text{aux}} = N \sum_{i=1}^{N} f_i r_i, \tag{3}$$

where f_i is the fraction of tokens dispatched to expert i, and r_i is the average router probability assigned to the expert. The final training loss, $\mathcal{L}$, averages the auto-regressive loss across K multi-resolution projections and combines it with the weighted auxiliary loss:

$$\mathcal{L} = \frac{1}{K} \sum_{j=1}^{K} \mathcal{L}_{\text{ar}} \left(\mathbf{X}_{t+1:t+p_j}, \hat{\mathbf{X}}_{t+1:t+p_j} \right) + \alpha \mathcal{L}_{\text{aux}}, \tag{4}$$

where p_j is the forecast horizon for the j-th projection and α is a scaling coefficient.

Model Configuration. We consider two model sizes in this work, demonstrating the scalability of our approach. TimeSqueeze $_{\text{base}}$ has a total of 117M parameters with 54M active parameters, while TimeSqueeze $_{\text{large}}$ contains 469M total parameters with 216M active parameters. Both models are trained for 100,000 steps with a batch size of 256 and a maximum context length of 2048, corresponding to 500K time points per iteration and a total of 50B time steps during pretraining. Finally, for the patching and unpatching modules, we target an average compression rate of 4 in TimeSqueeze by setting the threshold factor $\tau = 0.3$, and limiting the maximum patch size to 8, balancing computational savings and information preservation. Further configuration details are provided in Appendix A.

4 Experimental Results

Baselines. Our primary objective is to demonstrate the efficiency and performance improvements of TimeSqueeze over point embedding models through dynamic context compression. We use TimeMoE as our baseline, and pretrain TimeSqueeze following the training scheme of [7], but using $8\times$ lesser data and $\approx 20\times$ less train time, as shown in Figure 2a. We forecast on four prediction horizons $\{96, 192, 336, 720\}$ but use the same context length of 512 in all cases. While, we study the point-forecasting performance of TimeSqueeze, but it can easily be extended to provide probabilistic forecasts by substituting the model's linear projection head with a probabilistic head. We assess model performance using the mean squared error (MSE) and mean absolute error (MAE), computed between the predicted values and the ground truth. For completeness, we also compare against Moirai-large [11], TimesFM [10], Moment [6], and Chronos [9], with results taken from [7].

4.1 Zero-shot forecasting

We first compare the zero-shot performance of TimeSqueeze $_{\text{base}}$ and TimeSqueeze $_{\text{large}}$ against Time-MoE$_{\text{base}}$ and $_{\text{large}}$ on the well-studied long-term forecasting benchmarks [3] and the Weather data [4]. These datasets were not included in the Time-300B dataset and not used for training the TimeSqueeze. Detailed zero-shot forecasting results are presented in Table 1, demonstrating that TimeSqueeze performs remarkably well, achieving a performance similar to that of Time-MoE. Further results for higher compression rates are provided in Appendix D.

Additional comparisons for TimeSqueeze against Time-MoE are presented in Section E. We note that the performance of TimeSqueeze $_{\text{large}}$ is slightly worse than TimeSqueeze $_{\text{base}}$ in some scenarios, likely due to the limited training budget.

4.2 In-distribution forecasting

We now measure the full-shot performance by finetuning TimeSqueeze on the train split of the same benchmarks. For finetuning, we choose a learning rate of 1e-4 and fine-tune the pretrained model for just one epoch. We compare the full-shot performance against [24, 25, 26, 8, 27], in addition to the finetuned version of Time-MoE$_{\text{base}}$. As seen from Table 2, TimeSqueeze still performs close to Time-MoE, and outperforms all other baselines considered.

Table 1: Performance comparison of zero-shot forecasting. **Bold** for best and underscore for 2nd best.

Models	Metrics	TimeSqueeze $_{\text{base}}$		TimeSqueeze $_{\text{large}}$		Time-MoE$_{\text{base}}$		Time-MoE$_{\text{large}}$		Moirai$_{\text{base}}$		TimesFM		Moment		Chronos$_{\text{large}}$	
		MSE	MAE	MSE	MAE	MSE	MAE	MSE	MAE	MSE	MAE	MSE	MAE	MSE	MAE	MSE	MAE
ETTh1	96	0.359	0.385	0.360	**0.379**	0.357	0.381	**0.350**	0.382	0.376	0.392	0.414	0.404	0.688	0.557	0.441	0.390
	192	0.400	0.410	0.402	0.407	0.388	0.412	**0.384**	0.404	0.417	0.413	0.465	0.434	0.688	0.560	0.502	0.424
	336	0.420	0.423	0.423	**0.412**	**0.411**	0.430	**0.411**	0.434	0.433	**0.428**	0.503	0.456	0.675	0.563	0.576	0.467
	720	0.428	0.446	0.441	0.448	**0.427**	0.455	0.449	0.477	0.447	**0.444**	0.511	0.481	0.683	0.585	0.835	0.583
	Avg.	0.402	0.416	0.407	0.414	**0.394**	0.419	0.400	0.420	0.417	**0.419**	0.473	0.443	0.683	0.566	0.588	0.466
ETTh2	96	**0.282**	0.346	0.290	0.355	0.305	0.359	0.302	0.354	0.294	**0.330**	0.315	0.349	0.342	0.396	0.320	0.345
	192	**0.349**	0.394	0.368	0.413	0.351	0.386	0.364	0.385	0.365	**0.375**	0.388	0.395	0.354	0.402	0.406	0.399
	336	0.379	0.422	0.405	0.447	0.391	0.418	0.417	0.425	0.376	**0.390**	0.422	0.427	**0.356**	0.407	0.492	0.453
	720	0.444	0.471	0.445	0.441	0.419	0.454	0.537	0.496	0.416	**0.433**	0.443	0.454	**0.395**	0.434	0.603	0.511
	Avg.	0.363	0.408	0.377	0.414	0.366	0.404	0.405	0.415	0.362	**0.382**	0.392	0.406	**0.361**	0.409	0.455	0.427
ETTm1	96	0.312	0.344	**0.304**	**0.334**	0.338	0.368	0.309	0.357	0.363	0.356	0.361	0.370	0.654	0.527	0.457	0.403
	192	0.372	0.385	0.358	**0.367**	0.353	0.388	**0.346**	0.381	0.388	0.375	0.414	0.405	0.662	0.532	0.530	0.450
	336	0.435	0.425	0.403	**0.396**	0.381	0.413	**0.373**	0.408	0.416	**0.392**	0.445	0.429	0.672	0.537	0.577	0.481
	720	0.547	0.494	0.486	0.444	0.504	0.493	0.475	0.477	0.460	**0.418**	0.512	0.471	0.692	0.551	0.660	0.526
	Avg.	0.417	0.412	0.388	**0.385**	0.394	0.415	**0.376**	0.406	0.406	**0.385**	0.433	0.418	0.670	0.536	0.555	0.465
ETTm2	96	0.181	0.275	**0.179**	0.272	0.201	0.291	0.197	0.286	0.205	0.273	0.202	**0.270**	0.260	0.335	0.197	0.271
	192	**0.248**	0.323	0.251	0.325	0.258	0.334	0.250	0.322	0.275	0.316	0.289	0.321	0.289	0.350	0.254	**0.314**
	336	**0.310**	0.363	0.319	0.368	0.324	0.373	0.337	0.375	0.329	0.350	0.360	0.366	0.324	0.369	0.313	**0.353**
	720	0.431	0.437	0.425	0.428	0.488	0.464	0.480	0.461	0.437	0.411	0.462	0.430	**0.394**	**0.409**	0.416	0.415
	Avg.	**0.292**	0.349	0.294	0.348	0.317	0.365	0.316	0.361	0.311	**0.337**	0.328	0.346	0.316	0.365	0.295	**0.338**
Weather	96	0.1671	0.2172	0.170	0.221	0.160	0.214	**0.159**	0.213	0.220	0.217	-	-	0.243	0.255	0.194	0.235
	192	0.2188	0.2690	0.224	0.275	**0.210**	0.260	0.215	0.266	0.271	0.259	-	-	0.278	0.329	0.249	0.285
	336	0.278	0.315	0.292	0.326	**0.274**	0.309	0.291	0.322	0.286	0.297	-	-	0.306	0.346	0.302	0.327
	720	0.364	0.372	0.409	0.396	0.418	0.405	0.419	0.400	0.373	0.354	-	-	**0.350**	0.374	0.372	0.378
	Avg.	**0.257**	0.293	0.274	0.305	0.265	0.297	0.271	0.300	0.287	0.281	-	-	0.294	0.326	0.279	0.306
Average		**0.346**	0.376	0.348	0.373	0.347	0.380	0.352	0.380	0.357	**0.361**	0.407	0.403	0.465	0.440	0.434	0.400

4.3 Efficiency Comparison

We now compare the training and inference efficiency of TimeSqueeze $_{\text{base}}$ with the point-embedding baseline Time-MoE$_{\text{base}}$ model in terms of GPU hours and memory utilization. All experiments were conducted on $2\times$ NVIDIA A100 80GB GPUs.

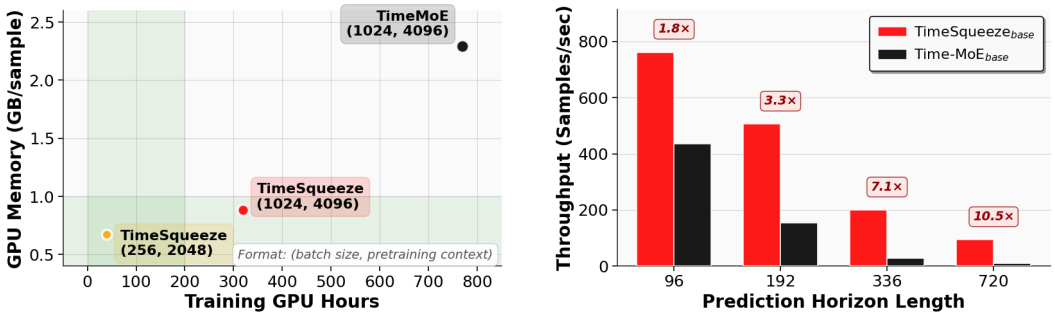

(a) (b)

Figure 2: Computational efficiency comparison between TimeSqueeze $_{\text{base}}$ and Time-MoE: (a) Training memory and time requirements across different batch sizes and context lengths. TimeSqueeze achieves comparable performance while reducing memory usage by $3.4\times$ and training time by $\approx 20\times$. (b) Inference throughput across prediction horizons. TimeSqueeze delivers up to $10.5\times$ higher throughput for longer prediction horizons.

In Figure 2a, we plot the pretraining time and memory required for different (batch size, context length) for Time-MoE and TimeSqueeze, when trained for $100,000$ iterations. When using $(1024, 4096)$, we see that TimeSqueeze uses $2.6\times$ less memory and $2.4\times$ less compute compared to Time-MoE. Furthermore, when running on a smaller budget, TimeSqueeze is trained with $(256, 2048)$, which uses $3.4\times$ less memory and $19.25\times$ less training time while still achieving performance comparable to Time-MoE, as shown in Table 1.

In Figure 2b, we plot the inference throughput for different forecasting horizons. We use a context length of 512 for TimeSqueeze and the original context lengths from [7] for Time-MoE. We see that TimeSqueeze scales more gracefully with respect to context length, showing up to $10.5\times$ faster inference for longer prediction horizons, making TimeSqueeze more suitable for on-device inference.

Table 2: Performance comparison of full-shot forecasting. **Bold** for best and underscore for 2nd best.

Models	Metrics	TimeSqueeze $_{\text{base}}$		Time-MoE$_{\text{base}}$		iTransformer		TimeMixer		TimesNet		PatchTST		DLinear	
		MSE	MAE	MSE	MAE	MSE	MAE	MSE	MAE	MSE	MAE	MSE	MAE	MSE	MAE
ETTh1	96	0.354	0.384	**0.345**	**0.375**	0.386	0.405	0.375	0.400	0.384	0.402	0.414	0.419	0.423	0.448
	192	0.397	0.412	**0.372**	**0.396**	0.441	0.436	0.436	0.429	0.421	0.429	0.460	0.445	0.471	0.474
	336	0.418	0.427	**0.389**	**0.412**	0.487	0.458	0.484	0.458	0.491	0.469	0.501	0.466	0.570	0.546
	720	0.423	0.454	**0.410**	**0.443**	0.503	0.491	0.498	0.482	0.521	0.500	0.500	0.488	0.653	0.621
	Avg.	0.398	0.419	0.379	0.406	0.454	0.447	0.448	0.442	0.454	0.450	0.468	0.454	0.529	0.522
ETTh2	96	**0.274**	**0.336**	0.276	0.340	0.297	0.349	0.289	0.341	0.340	0.374	0.302	0.348	0.745	0.584
	192	0.337	0.379	**0.331**	**0.371**	0.380	0.400	0.372	0.392	0.402	0.414	0.388	0.400	0.877	0.656
	336	**0.373**	0.408	**0.373**	**0.402**	0.428	0.432	0.386	0.414	0.452	0.541	0.426	0.433	1.043	0.731
	720	0.417	0.449	**0.404**	**0.431**	0.427	0.445	0.412	0.434	0.462	0.657	0.431	0.446	1.104	0.763
	Avg.	0.350	0.393	0.346	0.386	0.383	0.406	0.364	0.395	0.414	0.496	0.386	0.406	0.942	0.683
ETTm1	96	0.289	**0.332**	**0.286**	0.334	0.334	0.368	0.320	0.357	0.338	0.375	0.329	0.367	0.404	0.426
	192	0.344	0.366	**0.307**	**0.358**	0.377	0.391	0.360	0.381	0.374	0.387	0.367	0.385	0.450	0.451
	336	0.398	0.396	**0.354**	**0.390**	0.426	0.420	0.390	0.404	0.410	0.411	0.399	0.410	0.532	0.515
	720	0.502	0.451	**0.433**	0.445	0.491	0.459	0.454	0.441	0.478	0.450	0.454	**0.439**	0.666	0.589
	Avg.	0.383	0.386	0.345	0.381	0.407	0.409	0.381	0.395	0.400	0.405	0.387	0.400	0.513	0.495
ETTm2	96	**0.168**	**0.256**	0.172	0.265	0.180	0.264	0.175	0.258	0.187	0.267	0.175	0.259	0.287	0.366
	192	**0.225**	**0.298**	0.228	0.306	0.250	0.309	0.237	0.299	0.249	0.309	0.241	0.302	0.414	0.392
	336	**0.278**	**0.335**	0.281	0.345	0.311	0.348	0.298	0.340	0.321	0.351	0.305	0.343	0.597	0.542
	720	**0.366**	**0.395**	0.403	0.424	0.412	0.407	0.391	0.396	0.408	0.403	0.402	0.400	1.730	1.042
	Avg.	**0.259**	0.321	0.271	0.335	0.288	0.332	0.275	0.323	0.291	0.332	0.280	0.326	0.757	0.610
Weather	96	0.152	**0.199**	**0.151**	0.203	0.154	0.208	0.163	0.209	0.172	0.220	0.177	0.218	0.158	0.230
	192	0.201	0.249	**0.195**	**0.246**	0.202	0.251	0.208	0.250	0.219	0.261	0.225	0.259	0.206	0.277
	336	0.259	0.297	**0.247**	0.288	0.252	**0.287**	0.251	**0.287**	0.280	0.306	0.278	0.297	0.272	0.335
	720	0.360	0.372	0.352	0.366	**0.302**	0.376	0.339	**0.341**	0.365	0.359	0.354	0.348	0.308	0.418
	Avg.	0.243	0.279	**0.236**	0.275	0.250	0.280	0.240	0.271	0.259	0.286	0.258	0.280	0.258	0.315
Average		0.327	0.360	**0.315**	**0.357**	0.356	0.375	0.342	0.365	0.364	0.394	0.356	0.373	0.600	0.525

4.4 Ablation Studies

We conduct systematic ablation studies to quantify the contributions of key components in TimeSqueeze. We use TimeSqueeze $_{\text{base}}$ for all ablation studies, which were trained using the same approach as described in Section 3.2. During inference, we use a context length of 512 for TimeSqueeze and the original context lengths used in [7] for Time-MoE.

4.4.1 Model Components

Dynamic vs. Fixed Patching. We compare our proposed relative deviation-based dynamic patching approach with fixed patching. For the fixed patching baseline with patch size 4, embeddings are uniformly downsampled by retaining every 4th element. Results show that dynamic patching consistently outperforms fixed patching by effectively focusing computational resources on information-rich segments rather than optimizing only for a compression rate at the risk of discarding critical intermediate samples. This underscores the importance of dynamic compression strategies for handling temporal heterogeneity in time-series data.

Mamba vs. Linear Encoder. To assess the importance of our SSM encoder-decoder, we replace it with simple linear embedding layers akin to the architectures used in Moirai [11] and TimesFM [10]. The SSM-based encoder achieves substantial gains over linear projections, confirming its suitability for capturing fine-grained temporal features and its inductive bias, which is beneficial for sequential compression.

Importance of Fine-Grained Features. We evaluate the contribution of preserving detailed temporal information by ablating the residual connection illustrated in Figure 1, relying solely on compressed features for forecasting. This modification results in noticeable performance degradation.

Positional Encoding Analysis. We investigate the role of preserving positional information by comparing absolute position embeddings of boundary elements with relative positional encodings applied to compressed embeddings. Removing absolute positional cues results in notable performance drops, highlighting the necessity of absolute temporal positioning to maintain temporal coherence in the reconstructed sequences.

Observation. Figure 3a shows the summary of these ablations, by plotting the average MSE across the five benchmarking datasets for a prediction horizon of 96. The results clearly indicate that the inductive bias of SSM, combined with the dynamic context-aware pruning of SSM embeddings, is crucial to achieving optimal performance, while the residual connection and the use of absolute position IDs play a minor role. The full results are included in Appendix F, Table 6.

4.4.2 Long-Context Pretraining

Recent studies show that pretraining with longer context lengths can improve inference performance even when using shorter contexts during deployment [2]. We investigate this by training TimeSqueeze with different maximum pretraining context lengths under a fixed token budget of approximately 50B tokens. All models are trained for 100,000 steps, with batch sizes adjusted to account for context length differences, while maintaining an inference context length of 512 tokens.

Figure 3b demonstrates that longer pretraining contexts consistently improve inference performance even when using a shorter inference context pf 512 always. This indicates that exposure to extended sequences during pretraining enables TimeSqueeze to develop more robust temporal representations that effectively transfer to shorter inference contexts. Notably, unlike Time-MoE, TimeSqueeze achieves strong inference performance with short contexts, despite being pretrained on longer sequences, significantly reducing computational overhead during deployment.

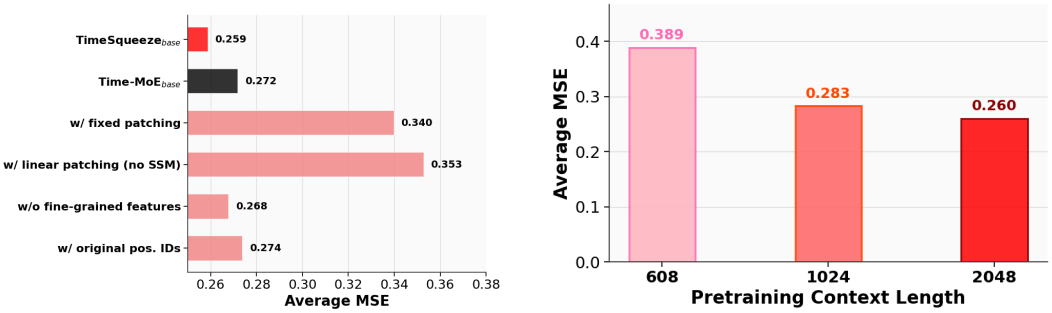

(a) (b)

Figure 3: Model analysis: (a) Average MSE across five benchmark datasets for prediction horizon 96 with different model components. (b) Effect of Pretraining Context Length on Forecasting Performance. Longer pretraining context translates to improved performance, even when the inference context remains fixed at 512.

5 Conclusion

We present **TimeSqueeze**, the first forecasting architecture with **dynamic, content-aware patching** that combines the temporal fidelity of point embedding models with the computational efficiency of patch-based approaches. TimeSqueeze employs a lightweight Mamba encoder for full-resolution feature extraction, followed by adaptive patching that assigns variable patch sizes based on temporal information density. Our mean deviation-based boundary detection enables data-driven compression decisions, producing variable-resolution representations that optimally allocate computational resources to where they provide the most significant forecasting benefit.

Our work opens several promising research directions. On the pretraining front, TimeSqueeze could benefit from scaling the number of parameters in the backbone and the amount of training data, similar to Time-MoE [7]. Further, the boundary detection mechanism could be enhanced through end-to-end learning in embedding spaces [17] or auxiliary model guidance [16]. TimeSqueeze's modular design enables integration with any transformer backbone, and combining it with advances in lightweight forecasting models [28] could yield greater computational savings.

References

[1] Tianyu Gao, Alexander Wettig, Howard Yen, and Danqi Chen. How to train long-context language models (effectively). *arXiv preprint arXiv:2410.02660*, 2024.

[2] Yong Liu, Guo Qin, Xiangdong Huang, Jianmin Wang, and Mingsheng Long. Timer-xl: Long-context transformers for unified time series forecasting. *arXiv preprint arXiv:2410.04803*, 2024.

[3] Haoyi Zhou, Shanghang Zhang, Jieqi Peng, Shuai Zhang, Jianxin Li, Hui Xiong, and Wancai Zhang. Informer: Beyond efficient transformer for long sequence time-series forecasting. In *Proceedings of the AAAI conference on artificial intelligence*, volume 35, pages 11106–11115, 2021.

[4] Haixu Wu, Jiehui Xu, Jianmin Wang, and Mingsheng Long. Autoformer: Decomposition transformers with auto-correlation for long-term series forecasting. *Advances in neural information processing systems*, 34:22419–22430, 2021.

[5] Tian Zhou, Ziqing Ma, Qingsong Wen, Xue Wang, Liang Sun, and Rong Jin. Fedformer: Frequency enhanced decomposed transformer for long-term series forecasting. In *International conference on machine learning*, pages 27268–27286. PMLR, 2022.

[6] Abdul Fatir Ansari, Lorenzo Stella, Caner Turkmen, Xiyuan Zhang, Pedro Mercado, Huibin Shen, Oleksandr Shchur, Syama Sundar Rangapuram, Sebastian Pineda Arango, Shubham Kapoor, et al. Chronos: Learning the language of time series. *arXiv preprint arXiv:2403.07815*, 2024.

[7] Xiaoming Shi, Shiyu Wang, Yuqi Nie, Dianqi Li, Zhou Ye, Qingsong Wen, and Ming Jin. Time-moe: Billion-scale time series foundation models with mixture of experts. *arXiv preprint arXiv:2409.16040*, 2024.

[8] Yuqi Nie, Nam H Nguyen, Phanwadee Sinthong, and Jayant Kalagnanam. A time series is worth 64 words: Long-term forecasting with transformers. *arXiv preprint arXiv:2211.14730*, 2022.

[9] Mononito Goswami, Konrad Szafer, Arjun Choudhry, Yifu Cai, Shuo Li, and Artur Dubrawski. Moment: A family of open time-series foundation models. *arXiv preprint arXiv:2402.03885*, 2024.

[10] Abhimanyu Das, Weihao Kong, Rajat Sen, and Yichen Zhou. A decoder-only foundation model for time-series forecasting. In *Forty-first International Conference on Machine Learning*, 2024.

[11] Gerald Woo, Chenghao Liu, Akshat Kumar, Caiming Xiong, Silvio Savarese, and Doyen Sahoo. Unified training of universal time series forecasting transformers. 2024.

[12] Ashish Vaswani, Noam Shazeer, Niki Parmar, Jakob Uszkoreit, Llion Jones, Aidan N Gomez, Łukasz Kaiser, and Illia Polosukhin. Attention is all you need. *Advances in neural information processing systems*, 30, 2017.

[13] Shiyang Li, Xiaoyong Jin, Yao Xuan, Xiyou Zhou, Wenhu Chen, Yu-Xiang Wang, and Xifeng Yan. Enhancing the locality and breaking the memory bottleneck of transformer on time series forecasting. *Advances in neural information processing systems*, 32, 2019.

[14] Albert Gu and Tri Dao. Mamba: Linear-time sequence modeling with selective state spaces. *arXiv preprint arXiv:2312.00752*, 2023.

[15] Kevin Slagle. Spacebyte: Towards deleting tokenization from large language modeling. *Advances in Neural Information Processing Systems*, 37:124925–124950, 2024.

[16] Artidoro Pagnoni, Ram Pasunuru, Pedro Rodriguez, John Nguyen, Benjamin Muller, Margaret Li, Chunting Zhou, Lili Yu, Jason Weston, Luke Zettlemoyer, et al. Byte latent transformer: Patches scale better than tokens. *arXiv preprint arXiv:2412.09871*, 2024.

[17] Sukjun Hwang, Brandon Wang, and Albert Gu. Dynamic chunking for end-to-end hierarchical sequence modeling. *arXiv preprint arXiv:2507.07955*, 2025.

[18] Olaf Ronneberger, Philipp Fischer, and Thomas Brox. U-net: Convolutional networks for biomedical image segmentation. In *International Conference on Medical image computing and computer-assisted intervention*, pages 234–241. Springer, 2015.

[19] Rewon Child. Very deep vaes generalize autoregressive models and can outperform them on images. In *International Conference on Learning Representations*, 2021.

[20] Jonathan Ho, Ajay Jain, and Pieter Abbeel. Denoising diffusion probabilistic models. *Advances in neural information processing systems*, 33:6840–6851, 2020.

[21] Yulun Wu, Louis McConnell, and Claudia Iriondo. Counterfactual generative modeling with variational causal inference. In *The Thirteenth International Conference on Learning Representations*, 2025.

[22] Peter J Huber. Robust estimation of a location parameter. In *Breakthroughs in statistics: Methodology and distribution*, pages 492–518. Springer, 1992.

[23] William Fedus, Barret Zoph, and Noam Shazeer. Switch transformers: Scaling to trillion parameter models with simple and efficient sparsity. *Journal of Machine Learning Research*, 23(120):1–39, 2022.

[24] Yong Liu, Tengge Hu, Haoran Zhang, Haixu Wu, Shiyu Wang, Lintao Ma, and Mingsheng Long. itransformer: Inverted transformers are effective for time series forecasting. *arXiv preprint arXiv:2310.06625*, 2023.

[25] Shiyu Wang, Haixu Wu, Xiaoming Shi, Tengge Hu, Huakun Luo, Lintao Ma, James Y Zhang, and Jun Zhou. Timemixer: Decomposable multiscale mixing for time series forecasting. *arXiv preprint arXiv:2405.14616*, 2024.

[26] Haixu Wu, Tengge Hu, Yong Liu, Hang Zhou, Jianmin Wang, and Mingsheng Long. Timesnet: Temporal 2d-variation modeling for general time series analysis. *arXiv preprint arXiv:2210.02186*, 2022.

[27] Ailing Zeng, Muxi Chen, Lei Zhang, and Qiang Xu. Are transformers effective for time series forecasting? In *Proceedings of the AAAI conference on artificial intelligence*, volume 37, pages 11121–11128, 2023.

[28] Yihang Wang, Yuying Qiu, Peng Chen, Yang Shu, Zhongwen Rao, Lujia Pan, Bin Yang, and Chenjuan Guo. Lightgts: A lightweight general time series forecasting model. *arXiv preprint arXiv:2506.06005*, 2025.

[29] Stephan Rasp, Peter D Dueben, Sebastian Scher, Jonathan A Weyn, Soukayna Mouatadid, and Nils Thuerey. Weatherbench: a benchmark data set for data-driven weather forecasting. *Journal of Advances in Modeling Earth Systems*, 12(11):e2020MS002203, 2020.

[30] Song Chen. Beijing multi-site air-quality data. *UCI Machine Learning Repository*, 10:C5RK5G, 2019.

[31] Yu Zheng, Xiuwen Yi, Ming Li, Ruiyuan Li, Zhangqing Shan, Eric Chang, and Tianrui Li. Forecasting fine-grained air quality based on big data. In *Proceedings of the 21th ACM SIGKDD international conference on knowledge discovery and data mining*, pages 2267–2276, 2015.

[32] Tung Nguyen, Jason Jewik, Hritik Bansal, Prakhar Sharma, and Aditya Grover. Climatelearn: Benchmarking machine learning for weather and climate modeling. *Advances in Neural Information Processing Systems*, 36:75009–75025, 2023.

[33] Rakshitha Godahewa, Christoph Bergmeir, Geoffrey I Webb, Rob J Hyndman, and Pablo Montero-Manso. Monash time series forecasting archive. *arXiv preprint arXiv:2105.06643*, 2021.

[34] Soukayna Mouatadid, Paulo Orenstein, Genevieve Flaspohler, Miruna Oprescu, Judah Cohen, Franklyn Wang, Sean Knight, Maria Geogdzhayeva, Sam Levang, Ernest Fraenkel, et al. Subseasonalclimateusa: A dataset for subseasonal forecasting and benchmarking. *Advances in Neural Information Processing Systems*, 36:7960–7992, 2023.

A Pretraining Configuration

The training configuration follows the same as Time-MoE: forecasting horizons are set to $\{1, 8, 32, 64\}$ in the output projection, and the auxiliary loss weighting factor α is 0.02. We optimize with AdamW using initial learning rate 1×10^{-3}, weight decay 0.1, $\beta_1 = 0.9$, and $\beta_2 = 0.95$. The learning rate scheduler employs a linear warmup for the first 10,000 steps, followed by cosine annealing to a minimum learning rate of 5×10^{-5}. Training is performed on 2 NVIDIA A100 80GB GPUs using BF16 precision, and the configurations for each model are described in detail in Table 3.

Table 3: Model configurations.

	Enc. Layers	Dec. Layers	d_{model}	d_{state}	d_{conv}	expand	Params
TimeSqueeze $_{\text{base}}$	2	2	384	128	4	4	4M
TimeSqueeze $_{\text{large}}$	2	2	768	128	4	4	16M

(a) Mamba encoder–decoder.

Model	Layers	Heads	Experts	K	d_{model}	d_{ff}	d_{expert}	Activated Params	Total Params
TimeSqueeze $_{\text{base}}$	12	12	8	2	384	1536	192	50M	113M
TimeSqueeze $_{\text{large}}$	12	12	8	2	768	3072	384	200M	453M

(b) Transformer backbone.

B Downsampling of Pretraining dataset

The original Time-300B dataset is heavily skewed by the Nature domain, which contributed to more than 90% of the dataset, as shown in Table 4.

Table 4: Key statistics of the pre-training dataset Time-300B from various domains.

	Energy	**Finance**	**Healthcare**	**Nature**	**Sales**	**Synthetic**	**Transport**	**Web**	**Other**	**Total**
# Seqs.	2,875,335	1,715	1,752	31,621,183	110,210	11,968,625	622,414	972,158	40,265	48,220,929
# Obs.	15.981 B	413.696 K	471.040 K	279.724 B	26.382 M	9.222 B	2.130 B	1.804 B	20.32 M	309.09 B
Percent %	5.17%	0.0001%	0.0001%	90.50%	0.008%	2.98%	0.69%	0.58%	0.006%	100%

And within the Nature domain, the 3 largest domains datasets contribute the most, as seen in Table 5.

Table 5: Key properties of Nature dataset from Time-300B..

Dataset	**Domain**	**Freq.**	**# Time Series**	**# Obs.**	**Source**
Weatherbench (Hourly)	Nature	H	3,984,029	74,630,250,518	[29]
Weatherbench (Daily)	Nature	D	301,229	3,223,513,345	[29]
Weatherbench (Weekly)	Nature	W	226,533	462,956,049	[29]
Beijing Air Quality	Nature	H	4,262	2,932,657	[30]
China Air Quality	Nature	H	17,686	4,217,605	[31]
CMIP6	Nature	6H	14,327,808	104,592,998,400	[32]
ERA5	Nature	H	11,940,789	93,768,721,472	[32]
Oikolab Weather	Nature	H	309	615,574	[33]
Saugeen	Nature	D	38	17,311	[33]
Subseasonal	Nature	D	17,604	51,968,498	[34]
Subseasonal Precipitation	Nature	D	13,467	4,830,284	[34]
Sunspot	Nature	D	19	45,312	[33]
Temperature Rain	Nature	D	13,226	3,368,098	[33]
Weather	Nature	D	9,525	26,036,234	[6]

In order to reduce the bias from these 3 datasets, we downsample the top 3 datasets by 30% at random during pretraining, bringing down the total number of samples in the pretraining dataset from 309B to $\approx$120B.

C Training Tokens vs Performance

Figure 4 demonstrates that TimeSqueeze exhibits favorable scaling behavior, with performance consistently improving as the training budget increases from 10B to 50B tokens. This scaling trend aligns with observations in [7], indicating that TimeSqueeze can effectively leverage larger datasets and computational resources. The consistent performance gains across different training scales suggest that TimeSqueeze exhibits similar scaling behavior to Time-MoE but with significantly improved data and compute efficiency, positioning it as a promising candidate for even larger-scale pretraining regimes.

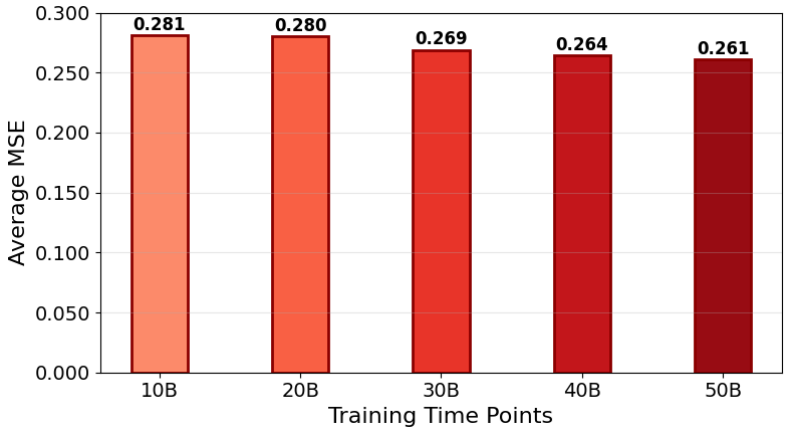

Figure 4: Performance scaling with training data size: Average MSE for 96-horizon forecasting across five benchmarks shows consistent improvement with increased training tokens.

D Compression Rate vs Performance

For the main results, we choose a moderate compression rate of $4\times$. We now compare the performance against two more variants of TimeSqueeze $_{\text{base}}$ trained with a target compression rate of $6\times$ and $8\times$, by adjusting the threshold factor to 0.4 and 0.45 respectively. And we plot the average MSE across the five datasets for prediction horizon 96. As expected, while the computational efficiency increases with higher compression, the performance also drops noticeably. techniques such as heirarchical compression

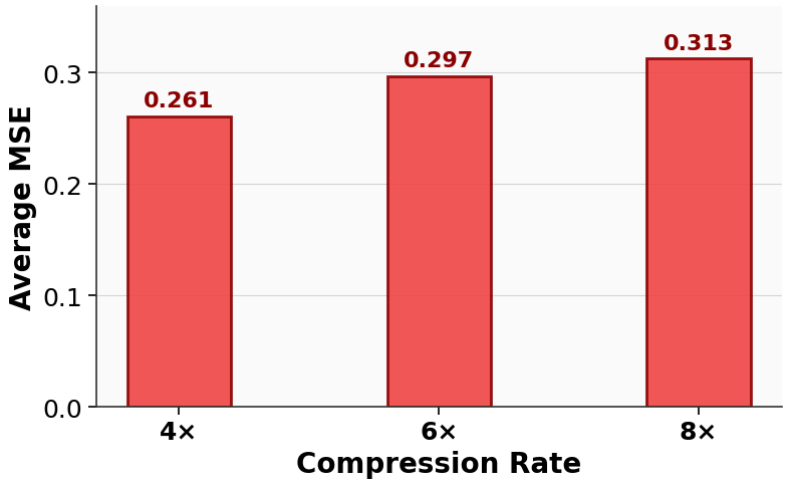

Figure 5: Performance scaling with training data size: Average MSE for 96-horizon forecasting across five benchmarks shows consistent improvement with increased training tokens.

E Performance for a Fixed Context Length

TimeSqueeze offers two key advantages over Time-MoE: First is the reduced token count to the Transformer backbone through dynamic compression. Further, TimeSqueeze also improves forecasting capability over longer horizons using shorter historical contexts, compared to point embedding models.

Our analysis demonstrates that for a fixed context length, TimeSqueeze significantly outperforms the point embedding baseline Time-MoE when predicting long-horizon forecasts. Figure 6 shows that for a given context length of 512, TimeSqueeze achieves a superior forecasting accuracy for the a horizon of 336. This improvement stems from our adaptive patching mechanism, which enables the model to extract more informative temporal patterns from limited historical data.

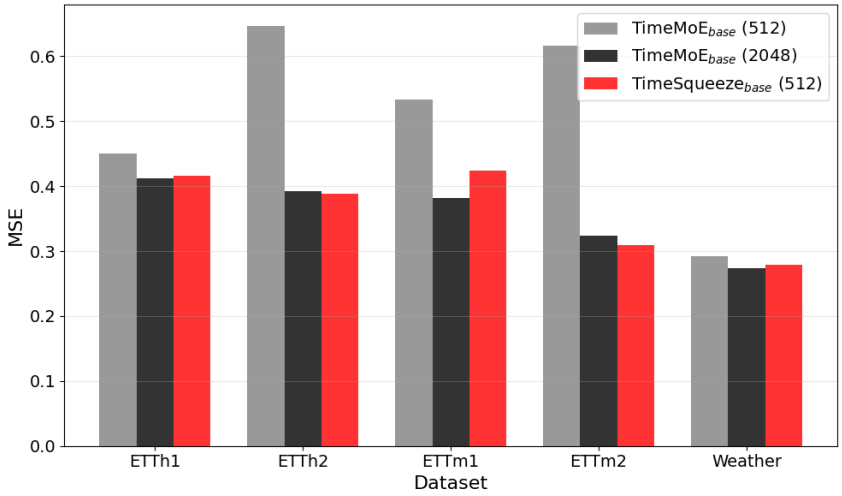

Figure 6: Performance comparison between TimeSqueeze and Time-MoE for a given context length for prediction horizon 336. TimeSqueeze noticeably outperforms the point-embedding baseline when the available context is limited.

F Additional Ablation Results

Table 6 contains the full et of results for the ablation studies presented in Section 4.4.

Table 6: Ablation study on zero-shot forecasting performance for prediction horizon 96.

Model / Variation	ETTh1		ETTh2		ETTm1		ETTm2		Weather		Average	
	MSE	MAE	MSE	MAE	MSE	MAE	MSE	MAE	MSE	MAE	MSE	MAE
TimeSqueeze $_{base}$	0.357	0.384	0.281	0.336	0.311	0.343	0.181	0.270	0.166	0.216	0.259	0.310
Time-MoE$_{base}$	0.357	0.381	0.305	0.359	0.338	0.368	0.201	0.291	0.160	0.214	0.272 (+5.0%)	0.323 (+4.2%)
TimeSqueeze w/ fixed patching	0.373	0.396	0.455	0.448	0.359	0.382	0.335	0.380	0.178	0.232	0.340 (+31.3%)	0.368 (+18.7%)
TimeSqueeze w/ linear patching (no SSM)	0.379	0.401	0.481	0.463	0.370	0.375	0.375	0.402	0.158	0.174	0.353 (+36.3%)	0.363 (+17.1%)
TimeSqueeze w/o fine-grained features	0.366	0.388	0.277	0.342	0.339	0.362	0.187	0.283	0.169	0.218	0.268 (+3.5%)	0.319 (+2.9%)
TimeSqueeze w/o original pos. IDs	0.375	0.393	0.291	0.358	0.346	0.363	0.191	0.293	0.169	0.219	0.274 (+5.8%)	0.325 (+4.8%)

F.1 Inference Context Length vs Performance

While longer context lengths generally provide more historical information for forecasting, the relationship between context length and performance is not monotonic. We investigate the effect of varying inference context lengths on forecasting accuracy by evaluating TimeSqueeze with context lengths ranging from 96 to 1536 tokens while keeping all other hyperparameters fixed.

Figure 7 reveals that performance initially improves as context length increases from 96 to 1536, reaching optimal performance around 512. However, further increasing the context length beyond this range leads to marginal performance degradation. This suggests that while additional historical

context can be beneficial up to a certain point, excessively long contexts may introduce noise or make it harder for the model to focus on the most relevant patterns.

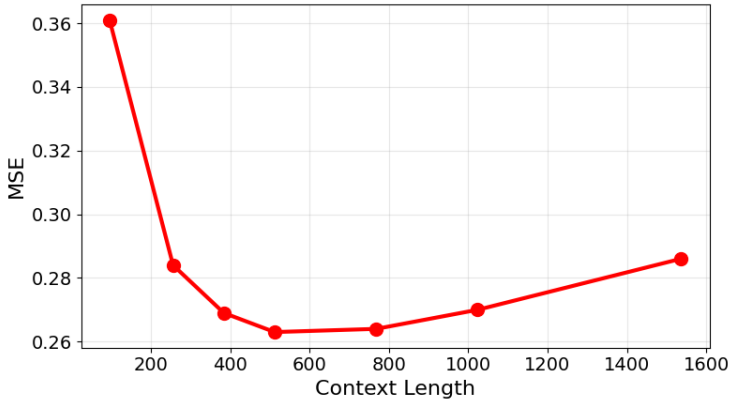

Figure 7: Forecasting performance improves with context length up to 512-800 tokens, then plateaus or slightly degrades.

G Visualization of patching

We provide the visualization of dynamic patches computed for an example segment of 128 samples from each of the evaluation datasets in Figures 8, 9, and 10. As we can see, weather dataset has slower variation in data resulting in larger patch sizes, whereas ETTm data has several regions with rapidly varying signal, resulting in much smaller patch sizes.

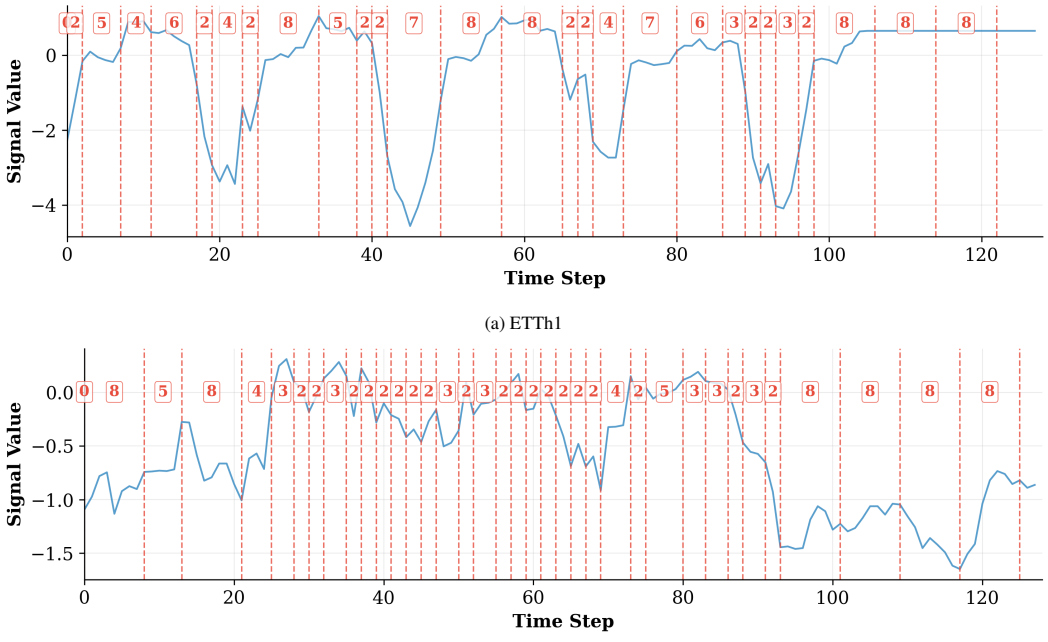

(a) ETTh1

(b) ETTh2

Figure 8: Example dynamic patch boundaries for ETTh1 and ETTh2 datasets.

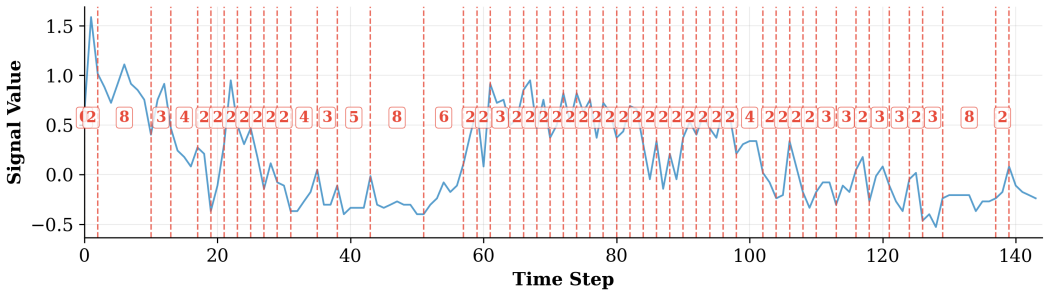

(a) ETTm1

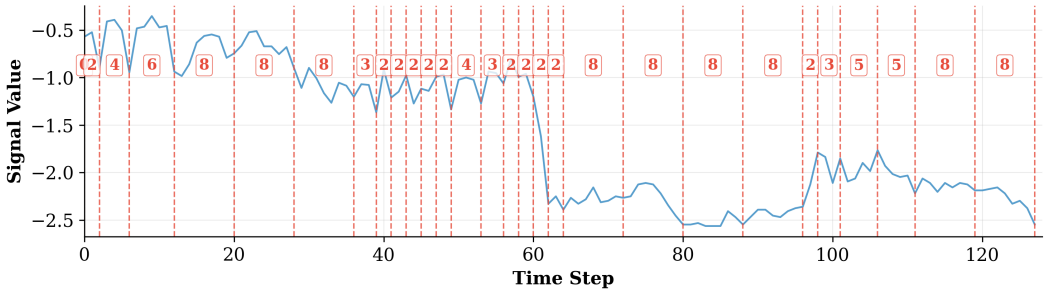

(b) ETTm2

Figure 9: Example dynamic patch boundaries for ETTm1 and ETTm2 datasets.

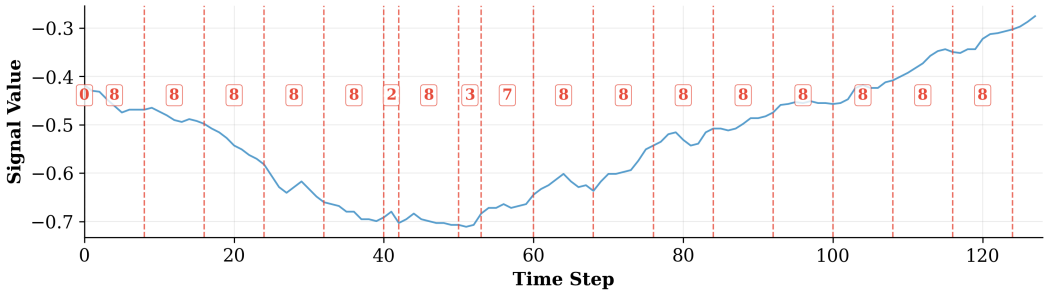

(a) Weather

Figure 10: Example dynamic patch boundaries for Weather dataset.

H Patch distribution

We provide the visualization of patch size distributions for each of the eval datasets in Figures 11. As we can see, weather dataset has slower variation in data resulting in larger avg patch size, whereas ETTm2 data has several regions with rapidly varying signal, resulting in much smaller patch sizes.

I Visualization of forecasts

We provide the visualization of forecasting results for an example segment of 128 samples from each of the evaluation datasets in Figures 12, 13, and 14. As observed, the Weather dataset exhibits relatively smooth and slowly varying dynamics, making forecasts easier to capture, whereas the ETTm datasets contain regions with rapid fluctuations, which pose greater challenges for accurate prediction.

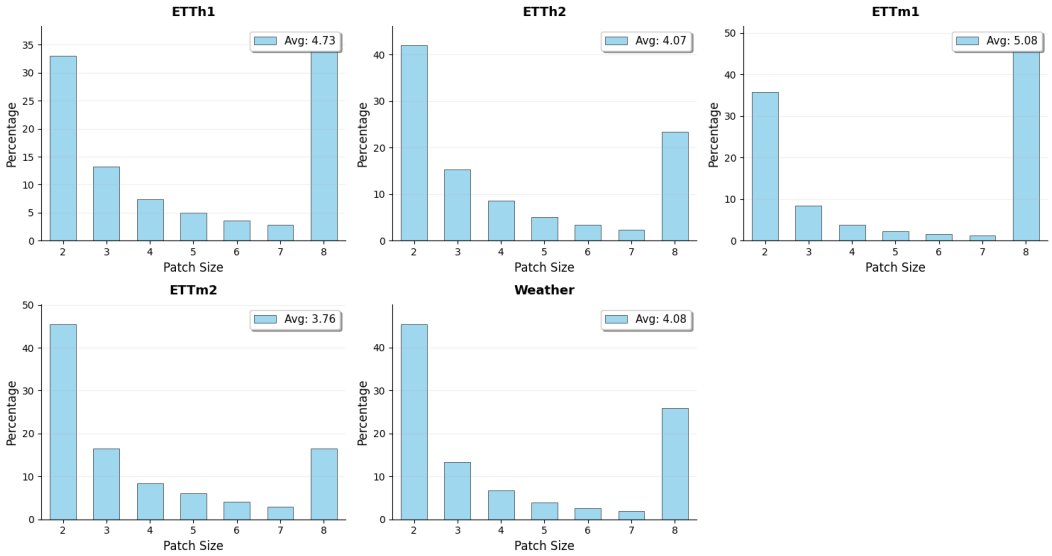

Figure 11: Distribution of patch sizes across eval datasets.

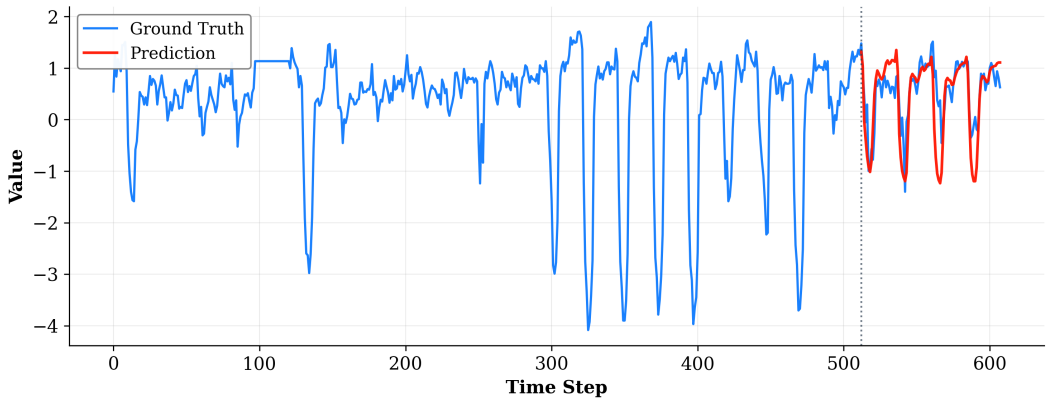

(a) ETTh1

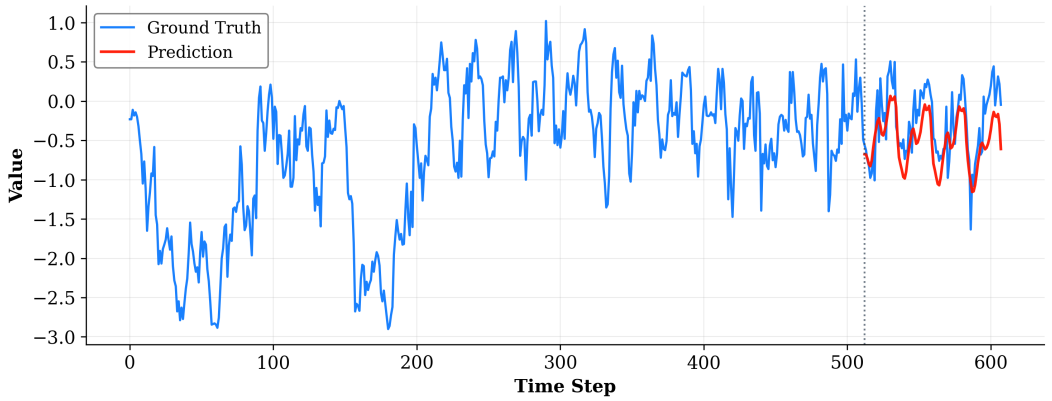

(b) ETTh2

Figure 12: Forecasting results on ETTh1 and ETTh2 datasets.

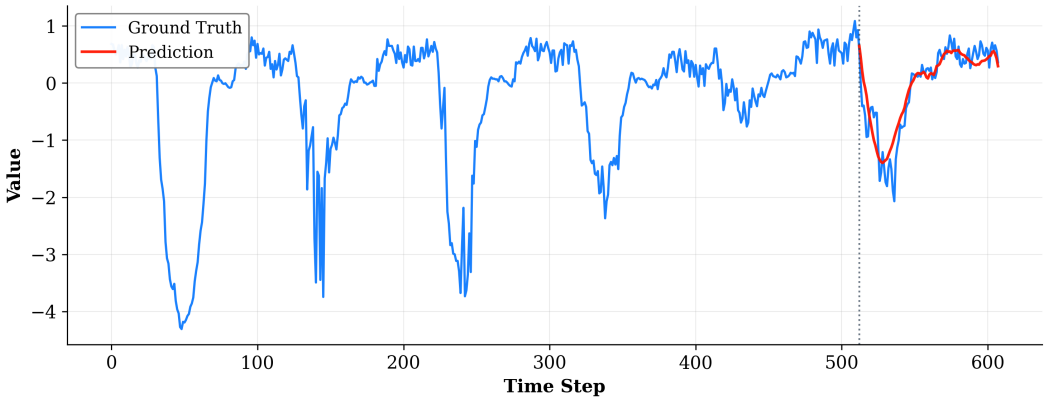

(a) ETTm1

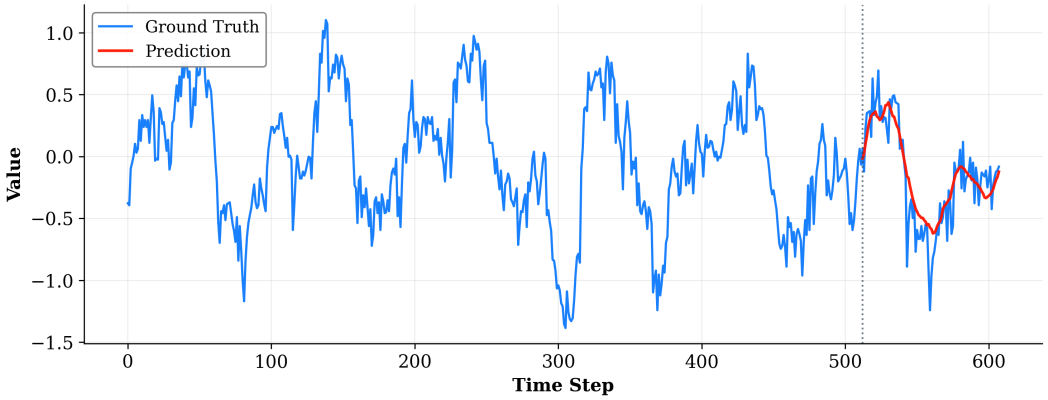

(b) ETTm2

Figure 13: Forecasting results on ETTm1 and ETTm2 datasets.

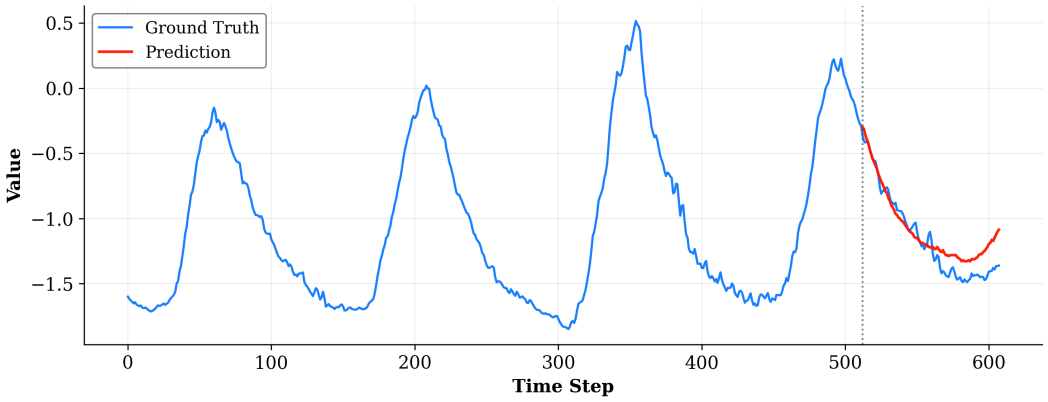

(a) Weather

Figure 14: Forecasting results on the Weather dataset.